

**This item is the archived peer-reviewed author-version of:**

$CO_2$  conversion in a gliding arc plasmatron : multidimensional modeling for improved efficiency

**Reference:**

Trenchev Georgi, Kolev St., Wang Weizong, Ramakers Marleen, Bogaerts Annemie.-  $CO_2$  conversion in a gliding arc plasmatron : multidimensional modeling for improved efficiency

The journal of physical chemistry : C : nanomaterials and interfaces - ISSN 1932-7455 - 121:44(2017), p. 24470-24479

Full text (Publisher's DOI): <https://doi.org/10.1021/ACS.JPCC.7B08511>

Full text (Publisher's DOI): <https://doi.org/10.1140/EPJC/S10052-017-5140-Y>

To cite this reference: <https://hdl.handle.net/10067/1471930151162165141>

# CO<sub>2</sub> Conversion in a Gliding Arc Plasmatron: Multi-Dimensional Modelling for Improved Efficiency

## Supporting information

G Trenchev<sup>1</sup>, St Kolev<sup>2</sup>, W Wang<sup>1</sup>, M Ramakers<sup>1</sup> and A Bogaerts<sup>1\*</sup>

<sup>1</sup>Research group PLASMANT, Department of Chemistry, University of Antwerp, Universiteitsplein 1, B-2610 Antwerp, Belgium

<sup>2</sup>Faculty of Physics, Sofia University, 5 James Bourchier Boulevard, 1164 Sofia, Bulgaria

### 1. Gas flow model

The flow calculation is performed by means of the CFD module in COMSOL<sup>1</sup>. This module includes several sub-modules for different applications. Typical CFD applications involve solving the Navier-Stokes equations for momentum and mass continuity. Simpler cases may use a Stokes flow approximation, where the inertial term is omitted. High-velocity and complex geometry problems should use turbulent models, which reduce the computational costs in comparison with methods like the Direct Numerical Simulation (DNS), which solves the full equations, or the Large Eddy Simulation, which solves only the most significant turbulent features in the flow completely. The turbulent model chosen in our study is the RANS (Reynolds-Averaged-Navier-Stokes) SST (Shear Stress Tensor) model<sup>2</sup>.

In general, all RANS models solve the following equations:

$$\nabla \cdot (\rho \overline{u_g}) = 0 \quad (1)$$

$$\rho (\overline{u_g} \cdot \nabla) \overline{u_g} = \nabla \cdot \left[ -p \vec{I} + (\mu + \mu_T) (\nabla \overline{u_g} + \nabla (\overline{u_g})^T) - \frac{2}{3} (\mu + \mu_T) (\nabla \cdot \overline{u_g}) \vec{I} - \frac{2}{3} \rho s_T \vec{I} \right] + \vec{F} \quad (2)$$

Equations 1 and 2 represent the mass and momentum continuity equations in the RANS model, where  $\rho$  stands for the gas density,  $\overline{u_g}$  is the gas flow velocity vector, superscript  $T$  stands for transposition,  $p$  is the gas pressure,  $\mu$  is the dynamic viscosity of the fluid,  $\mu_T$  is the turbulent viscosity of the fluid,  $s_T$  is the turbulent kinetic energy,  $\vec{I}$  is the unity tensor and  $\vec{F}$  is the body force vector, which in our case is not used. The viscous layer at the boundaries is fully resolved, i.e. the model is more accurate for the flow near the walls than in models where so-called wall functions are used, i.e., analytical solutions for the behavior near the walls. The model includes two more equations, in addition to equations 1 and 2, i.e., for the turbulent kinetic energy  $s_T$  and the specific dissipation  $\omega$ :

$$\rho (\overline{u_g} \cdot \nabla) s_T = \nabla \cdot [(\mu + \mu_T \sigma_k) \nabla s_T] + P - \beta_0 \rho \omega s_T \quad (3)$$

$$\rho (\overline{u_g} \cdot \nabla) s_T = \nabla \cdot [(\mu + \mu_T \sigma_\omega) \nabla \omega] + \frac{\gamma}{\mu_T} \rho P - \rho \beta_0 \omega^2 + 2(1 - f_{v1}) \frac{\sigma_{\omega 2}}{\omega} \nabla s_T \cdot \nabla \omega \quad (4)$$

Where:

$$P = \min(P_k 10 \rho \beta_0 S_T \omega) \quad (5)$$

$$P_k = \mu_T \left( \nabla \vec{u}_g : (\nabla \vec{u}_g + (\nabla \vec{u}_g)^T) - \frac{2}{3} (\nabla \cdot \vec{u}_g)^2 \right) - \frac{2}{3} \rho S_T \nabla \cdot \vec{u}_g \quad (6)$$

$$\mu_T = \frac{\rho a_1 S_T}{\max(a_1 \omega, S f_{v2})} \quad (7)$$

$$S = \sqrt{2 S_{ij} S_{ij}} \quad (8)$$

In equation (8), S stands for the characteristic magnitude of the mean velocity gradients.  $\beta_0$  is a model interpolation constant. In equation (7),  $f_{v2}$  stands for interpolation function:

$$f_{v2} = \tanh(\theta_2^2) \quad (9)$$

$$\theta_2 = \max\left(\frac{2\sqrt{S_T}}{\beta_0 \omega l_w^2}\right) \quad (10)$$

The boundary conditions implemented in this model are summarized in Table S1.

**Table S1.** Boundary conditions for the flow model.

Boundary	Expression	Note
Walls	$\vec{u}_g = 0$	Zero velocity
Inlet	$\vec{u} = -u_0 \vec{n}$	Velocity
Outlet	$\left[ -p \vec{I} + (\mu + \mu_T) (\nabla \vec{u}_g + (\nabla \vec{u}_g)^T) - \frac{2}{3} (\mu + \mu_T) (\nabla \cdot \vec{u}_g) \vec{I} - \frac{2}{3} \rho S_T \vec{I} \right] \vec{n} = -\widehat{p}_0 \vec{n}$	Pressure
Outlet	$-\widehat{p}_0 \leq p_0$	Suppress backflow

$\vec{n}$  is the normal vector,  $\vec{I}$  is the unity tensor,  $p_0$  is the atmospheric pressure,  $\widehat{p}_0$  is the adjusted pressure

A stationary solver with a wall distance  $l_w$  initialization is used to compute the model.

## 2. Turbulent heat transfer

The turbulent heat transfer is computed by enabling the multi-physics node in COMSOL<sup>1</sup>. The turbulent flow module (described above) is combined with the Heat Transfer module. In essence, a distribution of the turbulent heat conductivity is computed by the turbulent model output variables. Then, an effective heat conductivity, which combines the turbulent one with the static gas conductivity, is used in the heat transfer equation. The heat transfer equation is denoted as:

$$\rho C_p \frac{\partial T_g}{\partial t} + \rho C_p \vec{u}_g \cdot \nabla T_g - \nabla \cdot ((k_g + k_T) \nabla T_g) = Q \quad (11)$$

where  $C_p$  is the specific heat capacity of the gas,  $k_g$  is the temperature-dependent gas thermal conductivity (based on a material look-up table),  $k_T$  is the turbulent heat conductivity of the fluid,  $T_g$  is the gas temperature and  $Q$  accounts for the gas heating due to elastic and inelastic collisions between electrons and heavy particles in the plasma.

The Kays-Crawford model<sup>3</sup> accounts for the resulting turbulent heat conductivity. It is solved for the turbulent Prandtl number, which is the ratio of the momentum eddy diffusivity and heat transfer eddy diffusivity. It is expressed with the following equation:

$$Pr_T = \left( \frac{1}{2Pr_{T\infty}} + \frac{0.3}{\sqrt{Pr_{T\infty}}} \frac{C_p \mu_T}{k_g} - \left( 0.3 \frac{C_p \mu_T}{k_g} \right)^2 \left( 1 - e^{-k_g / (0.3 C_p \mu_T \sqrt{Pr_{T\infty}})} \right) \right)^{-1} \quad (12)$$

where  $Pr_T$  is the turbulent Prandtl number and  $Pr_{T\infty}$  is the turbulent Prandtl number at infinity ( $\sim 0.85$ ). For turbulent models, the turbulent heat conductivity is given as:

$$k_T = \frac{C_p \mu_T}{Pr_T} \quad (13)$$

The conductive heat flux in equation 5 is then defined using the sum of the gas thermal conductivity and the turbulent thermal conductivity:

$$q = -(k_g + k_T) \nabla T_g \quad (14)$$

In this way, turbulence acts as an enhancement to the gas thermal conductivity through intense eddy mixing, resulting in a higher effective value for heat conduction for the conditions of the considered discharge, i.e. heat transfer is dominated by turbulent effects.

### 3. 3D argon plasma model

The 3D plasma model is based on the simplified argon chemistry, presented in previous works<sup>4</sup>. This model is comparable with more complex chemistry models<sup>5</sup>. It is a fluid plasma model, built upon the assumption of a quasi-neutral plasma, i.e. ion and electron densities are equal. The model is constructed using the Math module in COMSOL. The following equation is solved for the ion density:

$$\frac{\partial n_i}{\partial t} + \nabla \cdot (-D_i \nabla n_i + \mu_i n_i \overrightarrow{E_{amb}}) + (\vec{u}_g \cdot \nabla) n_i = R_i \quad (15)$$

where  $n_i$  stands for the ion density,  $\mu_i$  stands for the ion mobility,  $\overrightarrow{E_{amb}}$  is the ambipolar electric field,  $\vec{u}_g$  is the gas flow velocity vector,  $D_i$  is the ion diffusion coefficient, and  $R_i$  stands for the ion production and loss rates due to chemical reactions. The electron density  $n_e$  is derived from the quasi-neutrality condition, which in this case is  $n_e = n_i$  since only a single type of ion is considered in the model. The average electron energy  $\bar{\epsilon}_e$  is calculated through:

$$\frac{\partial n_e \bar{\epsilon}_e}{\partial t} + \nabla \cdot (-\mu_{\epsilon,e} n_e \vec{E} - D_{\epsilon,e} \nabla (n_e \bar{\epsilon}_e)) + (\vec{u}_g \cdot \nabla) n_e \bar{\epsilon}_e = q_e \vec{E} \cdot \vec{G}_e + n_e \Delta \bar{\epsilon}_e + Q_{bg} \quad (16)$$

Where  $Q_{bg}$  stands for the stabilizing background heat source and the electron flux is derived from:

$$G_e = -D_e \nabla n_e - \mu_e n_e \overline{E_{amb}} \quad (17)$$

The terms  $\mu_{\varepsilon,e}$  and  $D_{\varepsilon,e}$  stand for the energy mobility and diffusion, respectively:

$$\mu_{\varepsilon,e} = \frac{5}{3} \mu_e \quad (18)$$

$$D_{\varepsilon,e} = \frac{2}{3} \mu_{\varepsilon,e} \bar{\varepsilon}_e \quad (19)$$

The balance for the excited species is solved as:

$$\frac{\partial n_*}{\partial t} + \nabla \cdot (D_* \nabla n_*) = R_* \quad (20)$$

The ambipolar electric field is solved as follows:

$$\overline{E_{amb}} = \frac{\nabla n_i (-D_e + D_i)}{n_i (\mu_i + \mu_e)} \quad (21)$$

Instead of the Poisson equation, the charge conservation equation is solved:

$$\nabla \cdot [\sigma_{pl} (-\nabla \varphi)] = 0 \quad (22)$$

where  $\sigma_{pl}$  stands for the plasma conductivity and  $\varphi$  stands for electric potential.

$$\sigma_{pl} = |q_e| (\mu_e n_e + \mu_i n_i) \quad (23)$$

A reduced set of electron collisions is used in the model, as presented in Table S2. The reaction rates are obtained from argon cross-sections with Bolsig+.

**Table S2.** Electron impact reaction set assumed in the model.

Reaction	Rate coefficient	Ref.
$e + Ar \rightarrow e + Ar$	BS <sup>a</sup>	6
$e + Ar \rightarrow e + Ar(4s)$	BS	6
$e + Ar(4s) \rightarrow 2e + Ar^+$	BS	6
$Ar^+ + e + Ar \rightarrow Ar + Ar$	$k \left( \frac{m^6}{s} \right) = 1.5 \times 10^{-40} \left( \frac{T_g}{300} \right)^{-2.5}$ <sup>b</sup>	5

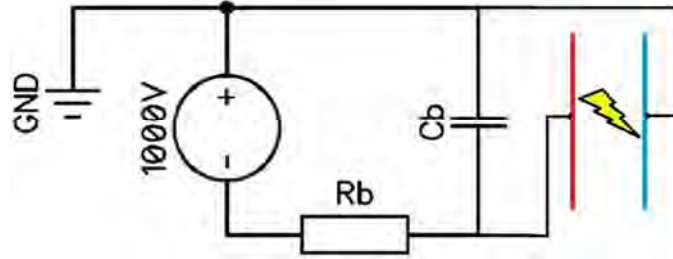
<sup>a</sup>Boltzmann solver, <sup>b</sup> $T_g$  in K

The boundary conditions implemented in the model are presented in table S3:

**Table S3.** Boundary conditions used in the model.

Boundary	Expression	Note
Walls	$-\vec{n} \cdot (-D_i \nabla n_i - \mu_i n_i \vec{E}_{amb}) = 0$	No flux
Walls	$-\vec{n} \cdot (-\mu_{\varepsilon,e} n_e \vec{E}_{amb} - D_{\varepsilon,e} \nabla (n_e \vec{\varepsilon}_e)) = 0$	No flux
Walls	$-\vec{n} \cdot (D_* \nabla n_*) = 0$	No flux
Walls	$-\vec{n} \cdot (-k \nabla T_g) = 0$	Adiabatic wall
Cathode	$U = -1000V$	Cathode voltage
Anode	$U = 0V$	Ground

The gliding arc current is calculated from a discharge control circuit featuring a ballast resistor.

**Figure S1.** Electrical scheme of the model with cathode (red) and anode (blue).

In figure S1, the ballast resistor limits the arc current, and it can be set in accordance with the desired current (i.e. 1320  $\Omega$  for 240 mA in the 3D argon model). The capacitor Cb (100pF) serves for reducing the voltage spikes. The electrodes are depicted in red (cathode) and blue (anode).

#### 4. 2D CO<sub>2</sub> plasma model

The CO<sub>2</sub> plasma model uses the principle described above, and its chemistry is adopted from <sup>7</sup>. The species included in the model are described in the main paper, while the electron impact reactions, ion reactions and vibrational energy transfer reactions are summarized in tables S4-S7.

**Table S4.** Electron impact reactions included in the model

Process	Reaction	Rate coefficient
Elastic collision <sup>a</sup>	$e + \text{CO}_2 \rightarrow e + \text{CO}_2$	EEDF
Ionization <sup>a</sup>	$e + \text{CO}_2 \rightarrow e + e + \text{CO}_2^+$	EEDF
Dissociative attachment <sup>b</sup>	$e + \text{CO}_2 \rightarrow \text{O}^- + \text{CO}$	EEDF
Dissociation <sup>b, d</sup>	$e + \text{CO}_2 \rightarrow e + \text{CO} + \text{O}$	EEDF
Electronic excitation <sup>a</sup>	$e + \text{CO}_2 \rightarrow e + \text{CO}_2e1$	EEDF
Vibrational excitation	$e + \text{CO}_2 \rightarrow e + \text{CO}_2v_a$	EEDF
Vibrational excitation	$e + \text{CO}_2 \rightarrow e + \text{CO}_2v_b$	EEDF
Vibrational excitation	$e + \text{CO}_2 \rightarrow e + \text{CO}_2v_c$	EEDF
Vibrational excitation	$e + \text{CO}_2 \rightarrow e + \text{CO}_2v_d$	EEDF
Vibrational excitation	$e + \text{CO}_2 \rightarrow e + \text{CO}_2v_i (i = 1-21)$	EEDF
Elastic collision	$e + \text{CO} \rightarrow e + \text{CO}$	EEDF
Dissociation	$e + \text{CO} \rightarrow e + \text{C} + \text{O}$	EEDF
Dissociative attachment	$e + \text{CO} \rightarrow \text{C} + \text{O}^-$	EEDF
Elastic collision <sup>a</sup>	$e + \text{O}_2 \rightarrow e + \text{O}_2$	EEDF
Dissociation <sup>b</sup>	$e + \text{O}_2 \rightarrow e + \text{O} + \text{O}$	EEDF
Ionization <sup>a</sup>	$e + \text{O}_2 \rightarrow e + e + \text{O}_2^+$	EEDF

Dissociative attachment <sup>b</sup>	$e + O_2 \rightarrow O + O^-$	EEDF
Attachment <sup>a</sup>	$e + O_2 + M \rightarrow M + O_2^-$	EEDF
Vibrational excitation	$e + O_2 \rightarrow e + O_2v_{1,2,3}$	EEDF
Attachment	$e + O + M \rightarrow M + O^-$	$1 \times 10^{-31}$
Electron-ion recombination	$e + CO_2^+ \rightarrow CO + O$	$2 \times 10^{-5} T_e^{-0.5} / T_g$
Electron-ion recombination	$e + CO_2^+ \rightarrow C + O_2$	$3.94 \times 10^{-7} T_e^{-0.4}$
Electron-ion recombination	$e + O_2^+ + M \rightarrow O_2 + M$	$1 \times 10^{-26}$
Electron-ion recombination	$e + O_2^+ \rightarrow O + O$	$6 \times 10^{-7} T_e^{-0.5} T_g^{-0.5}$

<sup>a</sup>Same cross section used for reactions of  $CO_2v_i$ , and idem for  $O_2v_i$ .

<sup>b</sup>Cross section also used for reactions of  $CO_2vi$ , and for  $O_2v_i$ , but modified by lowering the energy threshold by the excited state energy.

<sup>c</sup>Cross section also used for reactions of  $CO_2vi$ , but scaled and shifted in energy using Fridman's approximation <sup>8</sup>.

<sup>d</sup>Dissociation through electron impact excitation with 7.0 eV threshold.

Most rate coefficients are calculated from the cross sections and the electron energy distribution function, calculated in BOLSIG+, as indicated in the table by EEDF. Some rate coefficients (e.g. for electron-ion recombination) are directly adopted from literature. They are expressed in ( $cm^3 \cdot s^{-1}$ ) or ( $cm^6 \cdot s^{-1}$ ) for the two-body and three-body reactions, respectively.  $T_e$  is in eV and  $T_g$  is in K.

**Table S5.** Ion reactions included in the model

Process	Reaction	Rate coefficient
Recombination	$O^- + CO_2 + M \rightarrow CO_3^- + M$	$9.0 \times 10^{-29}$
Electron detachment	$O^- + CO \rightarrow CO_2 + e$	$5.5 \times 10^{-10}$
Electron detachment	$CO_3^- + CO \rightarrow 2CO_2 + e$	$5.0 \times 10^{-13}$
Recombination	$CO_3^- + CO_2^+ \rightarrow 2CO_2 + O$	$5.0 \times 10^{-7}$
Electron detachment	$O^- + M \rightarrow e + O + M$	$4.0 \times 10^{-12}$
Electron detachment	$O^- + O \rightarrow e + O_2$	$2.3 \times 10^{-10}$
Charge transfer	$O_2^- + O \rightarrow O^- + O_2$	$3.3 \times 10^{-10}$
Electron detachment	$O_2^- + O_2 \rightarrow O_2 + O_2 + e$	$2.18 \times 10^{-18}$
Electron detachment	$O_2^- + M \rightarrow O_2 + M + e$	$2.70 \times 10^{-10} (T_g/300)^{0.5} \exp(-5590/T_g)$
Charge transfer	$O + CO_3^- \rightarrow CO_2 + O_2^-$	$8.0 \times 10^{-11}$
Recombination	$O_2^- + CO_2^+ \rightarrow CO + O_2 + O$	$6.0 \times 10^{-7}$
Charge transfer	$O_2 + CO_2^+ \rightarrow CO_2 + O_2^+$	$5.3 \times 10^{-11}$
Charge transfer	$O + CO_2^+ \rightarrow CO + O_2^+$	$1.64 \times 10^{-10}$
Recombination	$O_2^+ + CO_3^- \rightarrow CO_2 + O_2 + O$	$3.0 \times 10^{-7}$
Recombination	$O_2^+ + O_2^- \rightarrow O_2 + O_2$	$2.0 \times 10^{-7}$
Recombination	$O_2^+ + O_2^- \rightarrow O_2 + O + O$	$4.2 \times 10^{-7}$
Recombination	$O_2^+ + O_2^- + M \rightarrow O_2 + O_2 + M$	$2.0 \times 10^{-25}$
Recombination	$O_2^+ + O^- \rightarrow O_2 + O$	$1.0 \times 10^{-7}$
Recombination	$O_2^+ + O_2^- \rightarrow O_2 + O + O$	$2.6 \times 10^{-8}$

$M$  represents any neutral species taken into account in the model. The same rate coefficient is used for every species. The rate coefficients are in ( $cm^3 \cdot s^{-1}$ ) or ( $cm^6 \cdot s^{-1}$ ) for the two-body and three-body reactions, respectively.

**Table S6.** Vibrational energy transfer reactions included in the model

Process	Reaction	Rate coefficient
VT relaxation <sup>a</sup>	$CO_2v_{a,b,c,d} + M \rightarrow CO_2 + M$	$7.14 \times 10^{-8} \exp(-177/T_g^{-1/3} + 451/T_g^{-2/3})$
VT relaxation <sup>a,b</sup>	$CO_2v_l + M \rightarrow CO_2v_a + M$	$0.43 \exp(-407/T_g^{-1/3} + 824/T_g^{-2/3})$
VT relaxation <sup>a,b</sup>	$CO_2v_l + M \rightarrow CO_2v_b + M$	$0.86 \exp(-404/T_g^{-1/3} + 1096/T_g^{-2/3})$
VT relaxation <sup>a,b</sup>	$CO_2v_l + M \rightarrow CO_2v_c + M$	$1.43 \times 10^{-5} \exp(-252/T_g^{-1/3} + 685/T_g^{-2/3})$
VV relaxation	$CO_2v_i + CO_2 \rightarrow CO_2v_{i-l} + CO_2v_{a,b} \quad (i \geq 2)$	$2.13 \times 10^{-5} \exp(-242/T_g^{-1/3} + 633/T_g^{-2/3})$
VV relaxation <sup>c</sup>	$CO_2v_i + CO_2v_j \rightarrow CO_2v_{i-l} + CO_2v_{j+l} \quad (20 \geq j \geq 0)$ $(21 \geq i \geq 1)$	$1.80 \times 10^{-11} \exp(24.7/T_g^{-1/3} - 65.7/T_g^{-2/3})$

VV relaxation <sup>a,c</sup>	$O_2v_i + M \rightarrow O_2v_{i-1} + M$	$(i = 1, 2, 3)$	$7.99 \times 10^{-5} \exp(-320/T_g^{-1/3} + 615/T_g^{-2/3})$
------------------------------	---	-----------------	--

<sup>a</sup>M represents any neutral species taken into account in the model. The same rate coefficient is used for every species.

<sup>b</sup>These reactions are also taken into account for  $v_i$  ( $i > 1$ ), but then they are not considered separately, and the rate coefficient is then taken as the sum of (i), (ii) and (iii), leading to level  $CO_2v_{i-1}$ , because for the higher levels, no individual symmetric mode levels are included in the model. See Kozák and Bogaerts<sup>9,10</sup> for more information.

<sup>c</sup> $v_0$  means the ground state of  $CO_2$  or  $O_2$ . The rate coefficients are in  $(cm^3 \cdot s^{-1})$  and  $T_g$  is in K. The rate coefficients are given for the reaction between ground state and first vibrational level, and they are scaled for the higher transitions.

VT: Vibrational – Translational; VV: Vibrational – Vibrational

**Table S7.** Neutral reactions included in the model

Process	Reaction	Rate coefficient
Neutral reaction	$CO_2 + M \rightarrow CO + O + M$	$4.39 \times 10^{-7} \exp(-65000/T_g)$
Neutral reaction	$CO_2 + O \rightarrow CO + O_2$	$7.77 \times 10^{-12} \exp(-16600/T_g)$
Neutral reaction	$CO + O + M \rightarrow CO_2 + M$	$8.20 \times 10^{-34} \exp(-1560/T_g)$
Neutral reaction	$CO + O_2 \rightarrow CO_2 + M$	$1.28 \times 10^{-12} \exp(-12800/T_g)$
Neutral reaction	$CO_2 + C \rightarrow CO + CO$	$1.00 \times 10^{-15}$
Neutral reaction	$O_2 + C \rightarrow CO + O$	$3.00 \times 10^{-11}$
Neutral reaction	$CO + M \rightarrow C + O + M$	$1.52 \times 10^{-4} \exp(T_g/298)^{-3.1} \exp(-12800/T_g)$
Neutral reaction	$C + O + M \rightarrow CO + M$	$2.14 \times 10^{-29} \exp(T_g/300)^{-3.08} \exp(-2114/T_g)$
Neutral reaction	$O + O + M \rightarrow O_2 + M$	$1.27 \times 10^{-32} \exp(T_g/300)^{-1} \exp(-170/T_g)$

The rate coefficients are in  $(cm^3 \cdot s^{-1})$  or  $(cm^6 \cdot s^{-1})$  for the two-body and three-body reactions, respectively. See Wang<sup>7</sup> and Kozák and Bogaerts<sup>9,10</sup> for more information.  $T_g$  is in K.

## References

1. Comsol Multiphysics, version 5.0; User's Guide, **2015**, [www.comsol.com](http://www.comsol.com) (accessed December 2015)
2. Menter, F. R.; Kuntz, M.; Langtry, R. Ten Years of Industrial Experience with the SST Turbulence Model, *Turbulence, Heat and Mass Transfer* **2003**, *4*, 625-632
3. Weigand, B.; An Extended Kays and Crawford turbulent Prandtl number model, *Int. J. Heat Mass Transf.* **1997**, *40*, 4191-4196
4. Trenchev, G.; Kolev, St.; Bogaerts, A. A 3D model of a reverse vortex flow gliding arc reactor, *Plasma Sources Sci. Tech.* **2016**, *25*, 035014
5. Kolev, St.; Bogaerts, A. A 2D model for a gliding arc discharge, *Plasma Sources Sci. Technol.* **2015**, *24*, 015025
6. BIAGI-v7.1 database, [www.lxcat.laplace.univ-tlse.fr](http://www.lxcat.laplace.univ-tlse.fr); Transcribed from SF Biagi's Fortran code MAGBOLTZ, <http://consult.cern.ch/writeup/magboltz> (accessed December 2015)
7. Wang, W.; Berthelot A.; Kolev, St.; Tu, X.; Bogaerts, A.  $CO_2$  conversion in a gliding arc plasma: 1D cylindrical discharge model, *Plasma Sources Sci. Technol.* **2016**, *25*, 065012
8. Fridman, A. *Plasma Chemistry*, Cambridge University Press, New York, US **2008**
9. Kozák, T.; Bogaerts, A. Splitting of  $CO_2$  by vibrational excitation in non-equilibrium plasmas: a reaction kinetics model, *Plasma Sources Sci. Technol.* **2014**, *23*, 045004
10. Kozák, T.; Bogaerts A. Evaluation of the energy efficiency of  $CO_2$  conversion in microwave discharges using a reaction kinetics model, *Plasma Sources Sci. Technol.* **2015**, *24*, 015024